


Article

Modeling and Synthesis of Alumina Whiskers Based on the Vapor Deposition Process

Wei Gong ¹, Xiang-Cheng Li ^{2,*}  and Bo-Quan Zhu ^{2,*}¹ Glarun Technology Co. Ltd., Nanjing 211106, China; gongwei1938@163.com² The State Key Laboratory of Refractories and Metallurgy, Wuhan University of Science and Technology, Wuhan 430081, China

* Correspondence: lixiangcheng@wust.edu.cn (X.-C.L.); z bqref@263.net (B.-Q.Z.)

Received: 28 September 2017; Accepted: 13 October 2017; Published: 17 October 2017

Abstract: This study simulated the bulk structure and surface energy of Al₂O₃ based on the density of states (DOS) and studied the synthesis and microstructure of one-dimensional Al₂O₃ whiskers. The simulation results indicate that the (001) surface has a higher surface energy than the others. The growth mechanism of Al₂O₃ whiskers follows vapor–solid (VS) growth. For the (001) surface with the higher surface energy, the driving force of crystal growth would be more intense in the (001) plane, and the alumina crystal would tend to grow preferentially along the direction of the (001) plane from the tip of the crystal. The Al₂O₃ grows to the shape of whisker with [001] orientation, which is proved both through modeling and experimentation.

Keywords: growth simulation; generation mechanism; Al₂O₃ whiskers; surface energy

1. Introduction

Compared with fibers with diameters in the millimeter or micrometer scale, Al₂O₃ whiskers with a sub-micrometer scale have the better advantages of high melting point, high specific strength, high specific modulus, high temperature oxidation resistance, and high chemical compatibility [1,2]. All these features give rise to the application of whiskers in the composite as a kind of excellent reinforcement phase in the fields of biology, aerospace, mechanics, polymers, and so on [3,4]. For example, D. Gomez-Garcia et al. [1] reported that ceramics with 3 wt. % Al₂O₃ whiskers exhibit comparable strength to pure ceramics, and the fracture toughness could be increased from 4.2 MPa·m^{1/2} to 5.6 MPa·m^{1/2}. S. Gonzalez-Lopez et al. [5] found that the addition of about 3 wt. % Al₂O₃ whiskers would double the flexural strength of alumina ceramics and benefit their application in biological fields. A. Ares et al. [6] determined that only 5 wt. % Al₂O₃ whiskers filler could increase the thermal stability of a polyethylene matrix by around 37% and possess excellent compatibility with the matrix. J. Corrochano et al. [7] added 10 vol. % Al₂O₃ whiskers in an aluminum matrix and enhanced the strength by five or six times. M.A. bdullah et al. [8] prepared Al₂O₃ whisker-reinforced zirconia ceramics and found that the rupture strength could reach 1325 MPa when 10 wt. % whiskers were introduced. At the same time, the Vickers hardness could be increased to 13.8 GPa. The above research work shows that Al₂O₃ whiskers definitely play a key role in ensuring excellent performance for composites or ceramics industries.

With the development of industrial manufacturing and material sciences, more and more researchers are focused on the preparation and application of such oxide whiskers as alumina. In 1957, W.W. Webb and W.D. Forgeng et al. [9] first fabricated alumina whiskers by heating mixtures of alumina and TiAl₃ at 1300–1450 °C for 2–24 h in a stream of hydrogen. Recently, many efforts have been made to obtain large-yield preparation of alumina whiskers to meet the requirements of industry applications. For example, C.N.R. Rao et al. [3] synthesized Al₂O₃ whiskers by heating a mixture

of Al and graphite powders in a zirconia boat under flowing Ar at 1300 °C for 6 h, and it grow along the [001] direction with high aspect ratios. E. Mudra et al. [2] used the sintering method to obtain Al₂O₃ electrospun fibers that were tens of micrometers in diameter. W.B. Dai et al. [4] obtained transition Al₂O₃ whiskers by the thermal decomposition of ammonium hexafluoroaluminate, and the whiskers' diameter was decreased to the near sub-micrometer scale. Y.H. Cui et al. [10] synthesized single crystal Al₂O₃ whiskers by an in situ method and found a screw dislocation growth mechanism followed by alumina whisker growth. The authors' previous research [11] reported that the synthesis of Al₂O₃ whiskers through the carbon-assisted method possessed the characteristics of easy operation and flexible reaction conditions. However, the above research only considers the synthesis of Al₂O₃ whiskers, but does not explore the simulation and growth mechanism of these whiskers.

In theory, a detailed and deep understanding of the simulation and modeling of one-dimensional alumina whiskers would play a key role in controlling the growth and manufacture experiments of these materials. Amongst these researching processes, the surface energy could determine their growth direction and the morphology according to crystal growing theory. To date, many researchers have studied the surface energy during the crystal growth process based on density functional theory (DFT) [12–15], and the corresponding synthesis mechanism of one-dimensional materials could theoretically be interpreted. For instance, Q.J. Liu et al. [16] calculated the surface energy of the (001) crystal face for cubic SrHfO₃, which indicated that—as the function of terminated slab—SrO was more stable than HfO₂. G.H. Chen et al. [17] also studied the electronic properties and structure of HfO₂ surfaces, and found that the (110) and (111) crystal faces could be terminated when a single oxygen layer was the most energetically favorable. X. Li et al. [18] studied the MgAl₂O₄ (111) surfaces and found that the O₂(Mg)- and Al(O)- terminated surfaces were of higher surface energy, which meant that it would easily interact with the other compounds and had the potential to grow in vacuum. P.L. Liu et al. [19] reported that the Zn-terminated ZnO (0001) polar surface with high surface energy was chemically active with the O₂ gas phase, leading to the rapid growth of nanotips along the *c*-axis direction. Therefore, the investigation of surface energy based on DFT would probably be successful in revealing the growth process and mechanism of one-dimensional whiskers.

Based on the above described research, the objective of this paper was to determine the relative surface stability and the preferred orientation Al₂O₃ through DFT under thermodynamic equilibrium conditions. Furthermore, the Al₂O₃ whiskers synthesis by the carbon-assisted method and its generation mechanism combined with surface energies was studied.

2. Simulation and Experimentation

The modeling and calculations in our work were performed with the density function theory (DFT) using plane-wave pseudopotential. The localized density approximation (LDA) with the Ceperley–Alder–Perdew–Zunger (CA–PZ) functional was implemented based on the Cambridge Serial Total Energy Package (CASTEP) code, and the model of Materials Studio software [20]. The ionic cores were represented by ultrasoft pseudo potentials for Al and O atoms, and the valence states of Al and O were denoted as Al 3s²3p¹ and O 2s²2p⁴, respectively. The cutoff energy of the plane-wave basis was 340 eV throughout the bulk and slab models. The special k-point sampling of the Monkhorst-Pack scheme was used to approximate the Brillouin zone integrations. This set of parameters could assure the total energy convergence of 5.0×10^{-6} eV/atom, the maximum force of 0.01 eV/Å, the maximum stress of 0.02 GPa, and the maximum displacement of 5.0×10^{-4} Å. In order to make the calculation of Al₂O₃ bulk, a mesh size of $6 \times 6 \times 2$ was used for k-point sampling.

Flake graphite (95.00 wt. % with $d_{50} = 0.088$ mm) and metallic Al powders (99.50 wt. %) were used as raw materials. The raw materials were mixed according to the mass ratio of Al:C = 3:7. The mixture was heated at 1300 °C for 3 h under an Ar atmosphere. The phase composition and crystalline of the as-synthesized sample (alumina whiskers) were analyzed by X-ray diffraction (XRD, X'Pert Pro, Philips, Amsterdam, The Netherlands) with a copper anode (Cu-K_{α1}, $\lambda = 0.15405$ nm) working at 40 kV and 40 mA, scanning in continuous mode at a rate of 2°·min^{−1}. The microstructure and morphology of alumina

whiskers were determined by scanning electron microscopy (FESEM, Nova 400 Nano SEM, FEI, Cambridge, UK) supported by energy-dispersive X-ray spectroscopy (EDS, INCA, IE350 penta FET X-3, Oxford, UK). The high resolution and crystalline structure were measured by transmission electron microscopy (TEM, JEM-2100 UHR, JEOL, Tokyo, Japan) and energy dispersive spectroscopy (EDS, Phoenix, Oxford, UK). Furthermore, the growth direction of alumina whiskers was depicted by TEM analysis.

3. Results and Discussion

3.1. Band Structure and Density of States

α -Al₂O₃ has a corundum structure (space group $R\bar{3}c$, No.167), which the O atoms stack in ABAB style, and Al atoms occupy the octahedral sites in the space group. The stable phase α -Al₂O₃ contains two units of Al₂O₃ in a rhombohedral representation. Before the surface calculations, the bulk model of Al₂O₃ was calculated and compared with experimental values in order to examining the reliability of the model. The calculated and theoretical values of the lattice parameters are listed in Table 1. It can be found that the optimized lattice parameter calculated by LDA is 5.12 Å, which is in good agreement with the experimental result of 5.14 Å [20] and other theoretical calculations [12–14].

Table 1. The calculated lattice parameters and theoretical values.

Sources	a (Å)	α (°)
Calculated	5.12	55.28
Reference [12]	5.06	55.31
Reference [13]	5.08	55.30
Reference [14]	5.14	55.17

The band structure and density of states (DOS) of Al₂O₃ are shown in Figure 1. From the band structure of Al₂O₃ in Figure 1a, it can be seen that the top of the valence band and bottom of the conduction band meet at the G point with a direct band gap of 6.704 eV, which is consistent with the previous theoretical results [21]. However, this value is smaller than its experimental value of 8.8 eV due to the LDA underestimating short-range repulsive interaction. Figure 1b–d show that the valence band of Al₂O₃ has three regions. The lower region between −20 eV to −15 eV is attributed to the O 2s state, and the middle region is composed of O 2p states hybridized with Al 3s and 3p states. The upper region is composed of Al 3s, Al 3p, and O 2p states, while the Al 3s and Al 3p states mainly contribute to the conduction band. The above results depict that Al–O bonding in Al₂O₃ reveals strong ionic characteristics. This agrees well with previous calculated results of Al₂O₃ based on DFT computational methods [22], and proves that the LDA calculations could be used to study the surface of Al₂O₃.

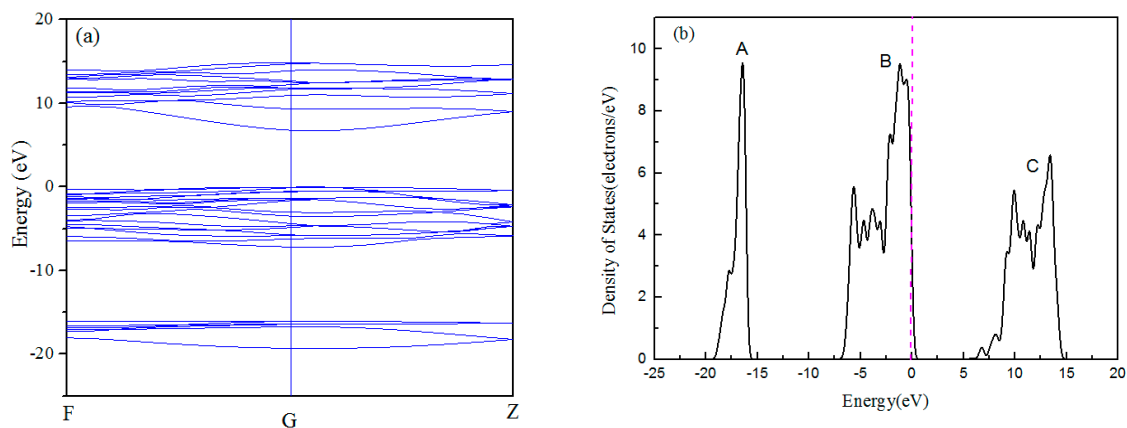


Figure 1. Cont.

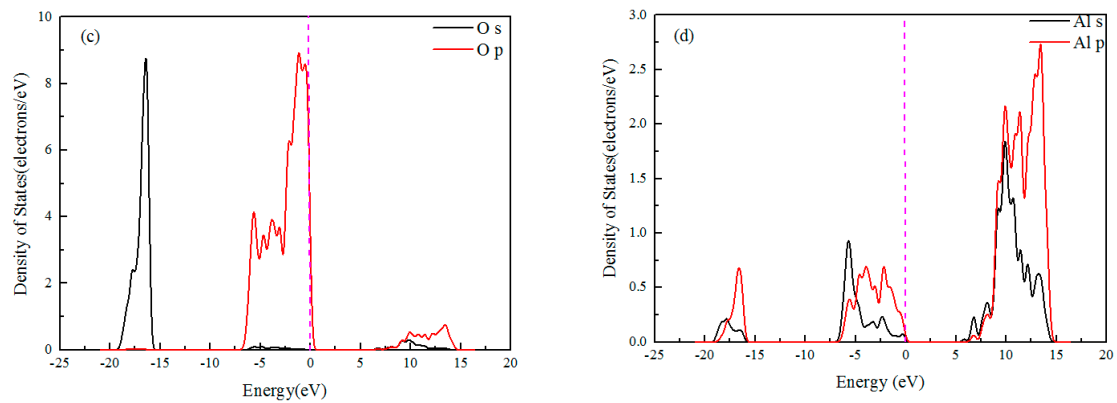


Figure 1. The band structure (a); density of states (DOS) (b); and projected DOS (c,d) of Al_2O_3 .

3.2. Surface Energies Calculation

In order to determine the relative surface stability and the preferred orientation of Al_2O_3 under thermodynamic equilibrium conditions, the state of the surface energy of the crystals becomes very important. To simulate the surface energies of Al_2O_3 , the slab model was used and the periodic boundary conditions were applied to the surface super cell under a vacuum region. The modeling of a slab of atomic layers is illustrated in Figure 2. The results showed that the vacuum layer is designed as 15 Å to avoid the interactions among periodic slabs of atomic layers. The unit cells of 1×1 are used for the low Miller index (i.e., (001), (110), and (113)) surface of Al_2O_3 in our calculations and modeling. For Al_2O_3 crystal, the surfaces of (001), (110), and (113) may be terminated and determined by Al or O layer. The atomic layers of 9 or 7 are used in the slab for the surface of Al_2O_3 here, as shown in Figure 2. The k-meshes of (001), (110), and (113) surfaces of Al_2O_3 in the calculations are $6 \times 6 \times 1$, $4 \times 5 \times 1$, and $3 \times 5 \times 1$.

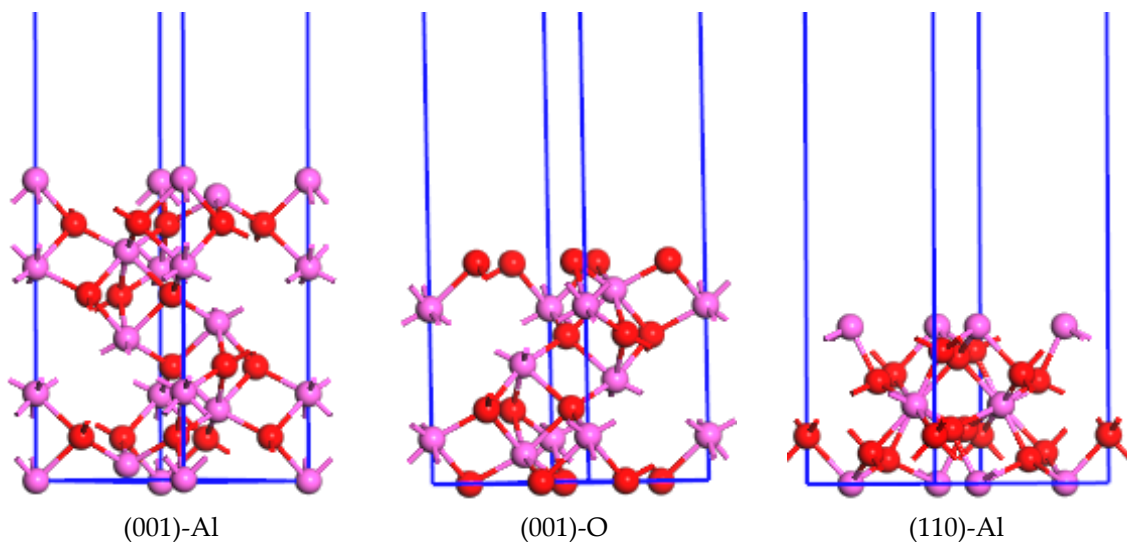


Figure 2. Cont.

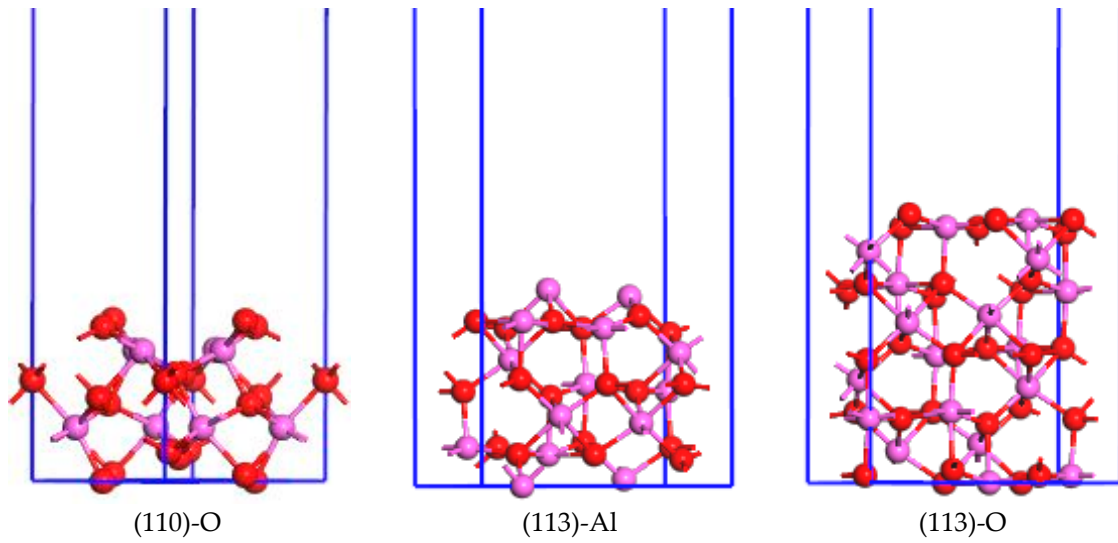


Figure 2. The ball and stick model for the surface structures of Al_2O_3 . “-Al” and “-O” mean the surfaces terminated by Al atoms and O atoms, respectively. Al atoms, O atoms.

We take the surface energy (E^{surf}) to represent the stability of various surfaces, and denote the surface energy as the cut-off energy of the crystal. For Al_2O_3 , E^{surf} is calculated as:

$$E^{\text{surf}} = \frac{1}{2A} \left[E_{\text{tot}}^{\text{slab}} - \frac{1}{2} N_{\text{Al}} E_{\text{tot}}^{\text{Al}_2\text{O}_3} - (N_{\text{O}} - \frac{3}{2} N_{\text{Al}}) \mu_{\text{O}} \right] \quad (1)$$

As explained in Reference [17], the value of $E_{\text{tot}}^{\text{slab}}$ is the total energy of the surface slab, and $E_{\text{tot}}^{\text{Al}_2\text{O}_3}$ refers to the energy of bulk Al_2O_3 per formula unit. The symbol of A is the surface area of the surface slab. N_{Al} and N_{O} are the number of Al atoms and O atoms in the slab, respectively. The excessive oxygen beyond stoichiometric Al_2O_3 units in the slab is denoted as $N_{\text{O}} - 3/2 N_{\text{Al}}$. μ_{O} varies between μ_{O}^0 and $\mu_{\text{O}}^{\text{Al}_2\text{O}_3}$. As we all know, the thermodynamically allowed chemical potential is key to study the dependence of surface stability on the environment. So, μ_{O}^0 is the chemical potential of oxygen and is taken as half of the total energy of one O_2 molecule. The relation between $\mu_{\text{O}}^{\text{Al}_2\text{O}_3}$ and $\mu_{\text{Al}}^{\text{Al}_2\text{O}_3}$ is given by a formula:

$$2\mu_{\text{Al}}^{\text{Al}_2\text{O}_3} + 3\mu_{\text{O}}^{\text{Al}_2\text{O}_3} = E_{\text{tot}}^{\text{Al}_2\text{O}_3}$$

The formation energy ($\Delta E_f^{\text{Al}_2\text{O}_3}$) of bulk Al_2O_3 is defined as:

$$\Delta E_f^{\text{Al}_2\text{O}_3} = E_{\text{tot}}^{\text{Al}_2\text{O}_3} - 2\mu_{\text{Al}}^0 - 3\mu_{\text{O}}^0$$

where μ_{Al}^0 is the chemical potential of Al, which is taken as the total energy of bulk Al. The variation range of μ_{O} can be obtained by:

$$\frac{1}{3} \Delta E_f^{\text{Al}_2\text{O}_3} + \mu_{\text{O}}^0 \leq \mu_{\text{O}} \leq \mu_{\text{O}}^0$$

In order to compare the stability of Al_2O_3 surfaces, the calculated surface energies for (001)-O, (001)-Al, (110)-O, (110)-Al, (113)-O, and (113)-Al versus the chemical potential of oxygen are plotted in Figure 3. Under oxygen-rich conditions, the surface energies of low Miller index surfaces of Al_2O_3 follow in the sequence of (001)-Al > (110)-Al > (113)-Al > (113)-O > (001)-O > (110)-O. Under oxygen-deficient conditions, the sequence converts to the trend of (001)-O > (110)-O > (113)-O > (001)-Al > (113)-Al > (110)-Al. The result indicates that the (110) surface is the most stable surface of Al_2O_3 . For the (001) surface with the higher surface energy, the driving force for crystal growth would be more intense in the (001) plane, and the alumina crystal would tend to grow preferentially along the

direction of the (001) plane from the tip of the crystal. As a consequence, the Al_2O_3 grew to the shape of a whisker with [001] orientation [19].

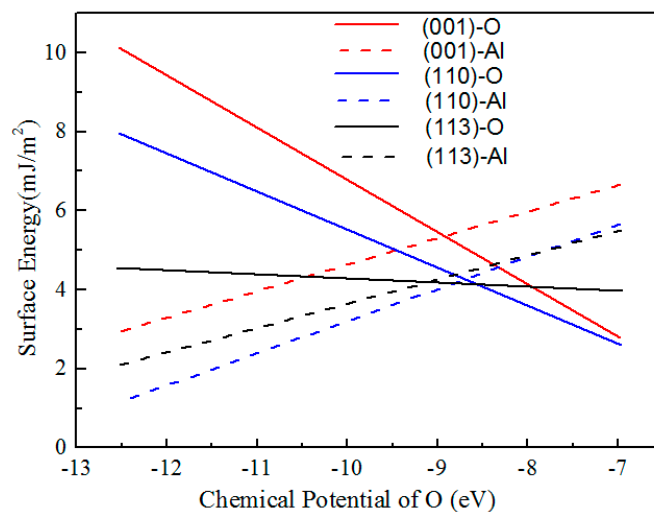


Figure 3. Surface energies for various surface of Al_2O_3 versus chemical potential of oxygen.

3.3. Phase Composition and Microstructure of the As-Synthesized Sample

According to the modeling and calculation of one-dimensional Al_2O_3 whiskers, detailed preparations were carried out. The XRD pattern of the as-synthesized sample heated at 1300 °C for 6 h is shown in Figure 4. The major phases in the as-synthesized samples are graphite, Al, and Al_2O_3 . The strongest diffraction peak of graphite is detected at 26.5°. Apart from graphite, the diffraction peaks at 25.49°, 35.05°, 37.68°, 43.25°, 52.48°, and 57.42° can be indexed as the (012), (104), (110), (113), (024), and (116) crystal planes of Al_2O_3 , respectively. The diffraction peaks of Al_2O_3 are the results of the metallic Al powders reacting with the remnant oxygen under high temperatures. This agrees with the authors' previous research [11].

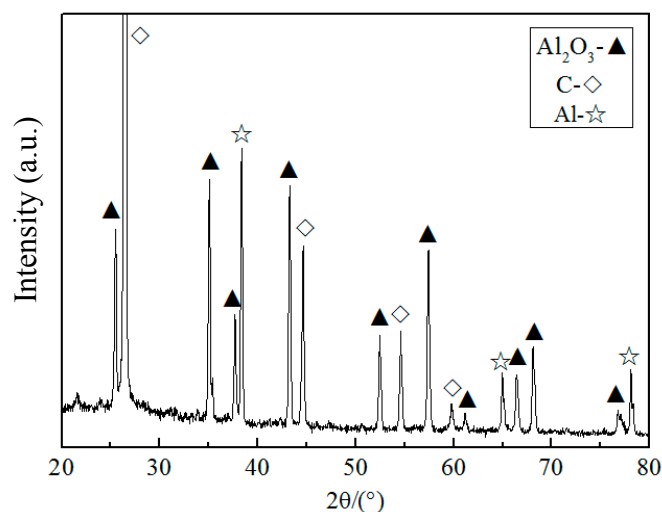


Figure 4. XRD pattern of the as-synthesized sample.

The SEM images and EDS spectrum of Al_2O_3 whiskers are shown in Figure 5. One-dimensional whiskers were formed in the as-synthesized sample, and the whiskers were 50–500 nm in diameter and hundreds of microns in length, as shown in Figure 5a,b. The EDS spectrum (Figure 5c) at point 1 of

Figure 5a are composed of three elements: O, Al, and carbon. The EDS spectrum clearly indicates that the whiskers have the composition of Al_2O_3 . This is in conformity with the Al_2O_3 phase determined by the XRD diffraction pattern (Figure 4). The high-magnification SEM images in Figure 5b show that the Al_2O_3 whiskers are smooth and flat, belonging to the hexagonal crystal system. There are no catalyst or liquid droplets at the ends of the whiskers, which means that the growth mechanism of Al_2O_3 whiskers follows the vapor–solid (VS) mechanism.

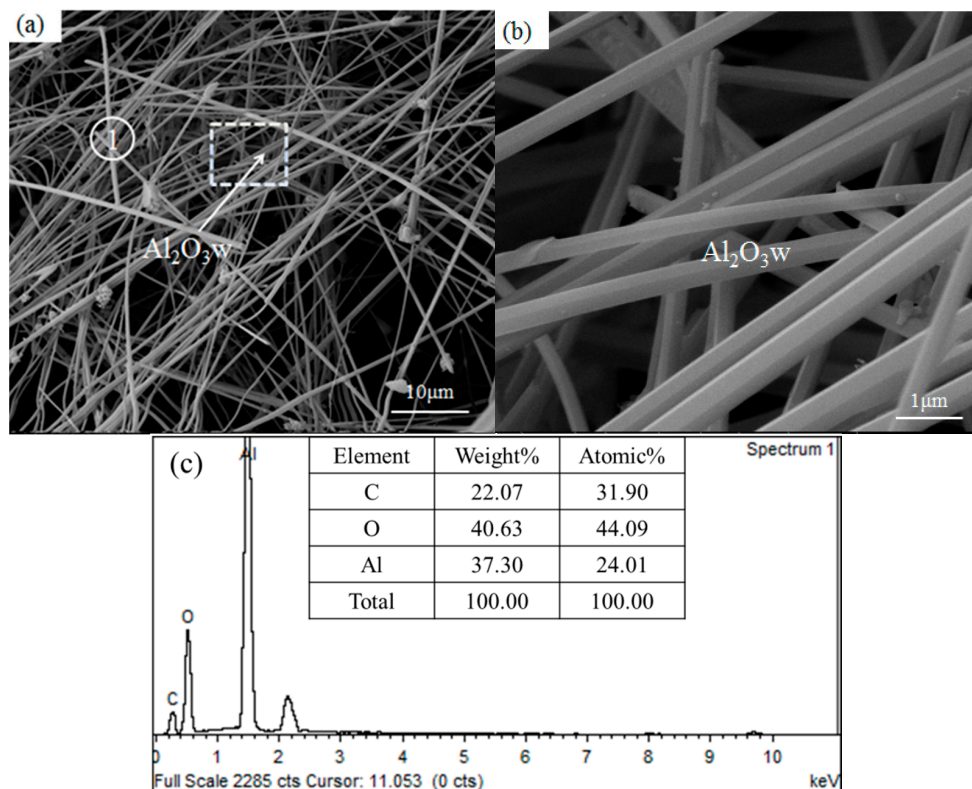


Figure 5. SEM images (a,b) and EDS spectrum (c) of the as-synthesized samples: $\text{Al}_2\text{O}_3\text{w}$ means Al_2O_3 whiskers.

In order to further explore the morphology of Al_2O_3 whiskers, a TEM analysis was conducted. The TEM image, selected area electron diffraction (SAED), and high-resolution TEM image of Al_2O_3 whiskers are shown in Figure 6. Figure 6a is the general TEM image of Al_2O_3 whiskers, with a diameter of about 100 nm. The SAED of the whiskers is depicted in Figure 6b. It could be found that the whiskers take on a single crystal with a hexagonal structure. According to the SAED, each diffraction spot corresponds to certain crystal face. The interplanar spacing of the two selected crystal faces and the angle (θ) of the two selected crystal faces were measured, respectively, as shown in Figure 6b. It reveals that the spacing is 0.21 nm for one crystal face (R_1) and 0.24 nm for the neighboring face (R_2). The angle (θ) of the two selected crystal faces is 27.94° . From the powder diffraction file (PDF) card 75–1865 for Al_2O_3 , the interplanar spacing for faces of (113) and (110) is respectively 0.2087 nm and 0.2382 nm, which correspond well with the measured R_1 and R_2 in Figure 6b. The angle between the two crystal faces of the hexagonal crystal could be also calculated from Equation (2):

$$\cos \theta = \frac{h_1 h_2 + k_1 k_2 + \frac{1}{2}(h_1 k_2 + h_2 k_1) + \frac{3a^2}{4c^2} l_1 l_2}{\sqrt{(h_1^2 + k_1^2 + h_1 k_1 + \frac{3a^2}{4c^2} l_1^2)(h_2^2 + k_2^2 + h_2 k_2 + \frac{3a^2}{4c^2} l_2^2)}} \quad (2)$$

where h , k , and l are defined as the lattice planes.

According to Equation (2), the angle of Al_2O_3 between the crystal face (113) and (110) is worked out to be 28° , consistent with the measured θ value in Figure 6b. So, the TEM analysis result confirms that the whiskers take on the Al_2O_3 phases. Furthermore, it can be seen in Figure 6b that the zone axis of Al_2O_3 whiskers is $[110]$, the diffraction spots along the whisker's axis is the crystal face (003), and its growth direction is parallel to $[001]$, namely, along the c -axis. This analysis is in agreement with the calculation results of the surface energy, shown in Figures 2 and 3. The HRTEM image of area 1 is shown in Figure 6c, which further proves that the Al_2O_3 whisker is a single crystal. The measured two lattice fringe spacing are 0.43 nm and 0.24 nm respectively, which are well matched with the (003) and (110) planes of the Al_2O_3 phases.

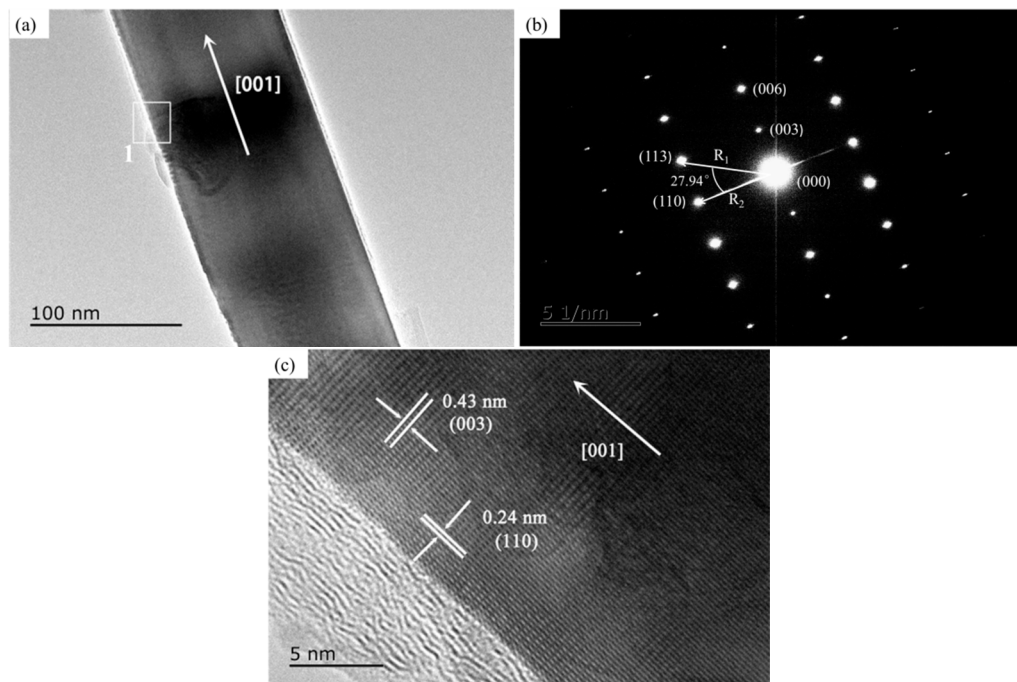


Figure 6. TEM image of Al_2O_3 whisker: (a) general TEM image; (b) SAED of Figure 6a; (c) high-resolution TEM.

3.4. The Generation Mechanism for Al_2O_3 Whiskers at High Temperatures

The generation mechanism of Al_2O_3 whiskers at 1300°C is investigated and simulated in Figure 7. The crystal morphology is determined using different crystal facet growth rates, which could be retarded or accelerated by such factors as impurities, intentionally introduced morphology modifiers, or temperature. In this experiment, the first step involves the melting of metallic Al powders and covering with a layer of graphite at 1300°C , as shown in Figure 7a. When the oxygen comes in contact with the graphite, the relevant reaction is given by:



Equation (3) takes place on the interface of graphite-Al powders. The sub-oxide AlO_x in the vapor state will continuously appear with the proceeding of the above reaction. Articles [23,24] also reported that the sub-oxide AlO_x in the carbon thermal reaction could be generated. Then, the sub-oxide AlO_x is oxidized to Al_2O_3 by oxygen in the Ar atmosphere, which forms Al_2O_3 nanocrystalline in the surface of the base crystal (shown in Figure 7c).

The surface energy's effect on the growth morphology is essential to control the growth and atoms state, as shown in Figures 2 and 3. According to the above surface energy calculation results, determining that the (001) surface has the higher surface energy, the driving force for crystal growth

would be more intense in the (001) plane, and the alumina crystal would tend to grow preferentially along the direction of the (001) plane from the tip of the crystal (shown in Figure 7c). As a result, the crystal sections of Al_2O_3 whiskers turn into the shape of whiskers with [001] orientation in hexagonal crystals, namely along the c -axis (shown in Figure 7d). These results agree with the experimental results in Figure 6. The growth mechanism of Al_2O_3 whiskers could be followed by the vapor–solid (VS) mechanism.

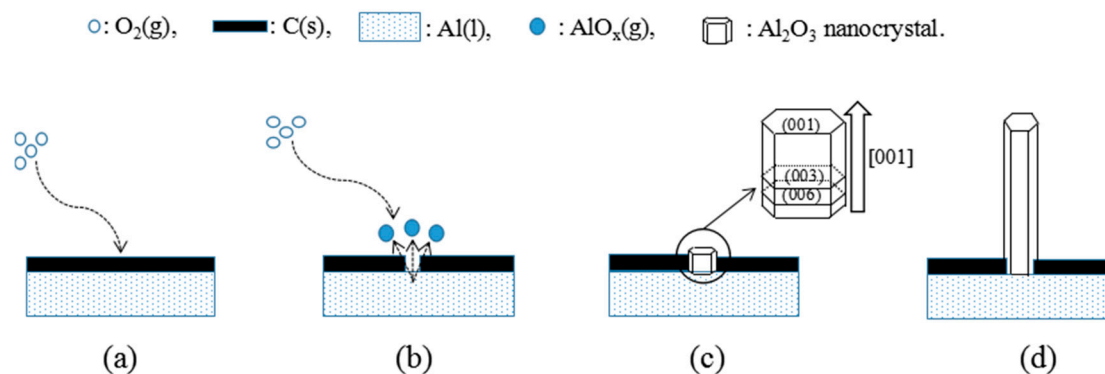


Figure 7. The generation mechanism of Al_2O_3 whiskers: (a) deposition of O_2 on molten Al layer; (b) generation of $\text{AlO}_x(\text{g})$; (c) growth on the direction of [001] and (d) the formation of Al_2O_3 whiskers.

4. Conclusions

- (1) Density of States calculation of Al_2O_3 showed that Al–O bonding exhibited strong ionic characteristics and the direct band gap between the top of the valence band and the bottom of the conduction band is 6.704 eV. The surfaces of (001), (110), and (113) would be terminated and determined by the Al or O layer.
- (2) Under oxygen-rich conditions, the surface energies of low Miller index surfaces of Al_2O_3 followed the sequence of (001)–Al > (110)–Al > (113)–Al > (113)–O > (001)–O > (110)–O. Under oxygen-deficient conditions, the sequence was converted to the trend of (001)–O > (110)–O > (113)–O > (001)–Al > (113)–Al > (110)–Al. The (001) surface possessed the higher surface energy.
- (3) The growth experiment of Al_2O_3 whiskers showed that the whiskers were 50–500 nm in diameter and hundreds of microns in length. The diffraction spots along the alumina whiskers' axis was the crystal face (003), and its growth direction was parallel to [001], namely, along the c -axis. This analysis was in agreement with the calculation and modeling results based on DOS.

Acknowledgments: The authors appreciate the financial support of the National Natural Science Foundation of China (Grant Nos. 51774218, 51674182 and 51602231).

Author Contributions: Wei Gong, Xiang-Cheng Li and Bo-Quan Zhu conceived and designed the experiments. Wei Gong performed the simulation and experiments as well as the paper writing. Xiang-Cheng Li and Bo-Quan Zhu contributed the data analysis, writing and financial support.

Conflicts of Interest: The authors declare no conflict of interest.

References

1. Tamura, Y.; Moshtaghioun, B.M.; Gomez-Garcia, D.; Rodríguez, A.D. Spark plasma sintering of fine-grained alumina ceramics reinforced with alumina whiskers. *Ceram. Int.* **2017**, *43*, 658–663. [[CrossRef](#)]
2. Mudra, E.; Streckova, M.; Pavlinak, D.; Medvecká, V.; Kovacik, D.; Kovalcikova, A.; Zubko, P.; Girman, V.; Dankova, Z.; Koval, V.; et al. Development of Al_2O_3 electrospun fibers prepared by conventional sintering method or plasma assisted surface calcination. *Appl. Surf. Sci.* **2017**, *415*, 90–98. [[CrossRef](#)]
3. Rao, C.; Gundiah, G.; Deepak, F.; Govindaraj, A.; Cheetham, A. Carbon-assisted synthesis of inorganic nanowires. *J. Mater. Chem.* **2004**, *14*, 440–450. [[CrossRef](#)]

4. Xu, M.; Wang, S.; Shen, F.; Ji, J.; Dai, W.J. Study on the influential factors for preparing transition alumina whiskers. *Alloys Compd.* **2017**, *695*, 2865–2869. [[CrossRef](#)]
5. Nevarez-Rascon, A.; Gonzalez-Lopez, S.; ACOSTA-TORRES, L.S.; NEVAREZ-RASCON, M.M.; Orrantia-Borunda, E. Synthesis, biocompatibility and mechanical properties of $\text{ZrO}_2\text{-Al}_2\text{O}_3$ ceramics composites. *Dent. Mater. J.* **2016**, *35*, 392–398. [[CrossRef](#)] [[PubMed](#)]
6. Ares, A.; Lasagabaster, A.; Abad, M.; Noguerol, R.; Cerecedo, C.; Valcárcel, V.; Caamano, J.; Guitián, F. Effects of silane functionalization of alumina whiskers on high-density polyethylene composites. *J. Compos. Mater.* **2014**, *48*, 3141–3151. [[CrossRef](#)]
7. Corrochano, J.; Cerecedo, C.; Valcárcel, V.; Lieblich, M.; Guitián, F. Whiskers of Al_2O_3 as reinforcement of a powder metallurgical 6061 aluminium matrix composite. *Mater. Lett.* **2008**, *62*, 103–105. [[CrossRef](#)]
8. Abdullah, M.; Ahmad, J.; Mehmood, M. Influence of Al_2O_3 whisker concentration on flexural strength of Al_2O_3 (w)– ZrO_2 (TZ-3Y) composite. *Ceram. Int.* **2012**, *38*, 6517–6523. [[CrossRef](#)]
9. Webb, W.; Forgeng, W. Growth and defect structure of sapphire microcrystals. *J. Appl. Phys.* **1957**, *28*, 1449–1454. [[CrossRef](#)]
10. Chu, Y.; Chen, P.; Tang, J.; Rao, P. Engineer in situ growth of $\alpha\text{-Al}_2\text{O}_3$ whiskers by axial screw dislocations. *Cryst. Growth Des.* **2017**, *17*, 1999–2005. [[CrossRef](#)]
11. Zhang, P.; Li, X.; Zhu, B. Influence of carbon source on the morphology of Al_2O_3 whiskers synthesized with a carbon assisted method. *Rare Met. Mater. Eng.* **2013**, *42*, 501–504.
12. Heid, R.; Strauch, D.; Bohnen, K.P.; Bohnen, K.P. Ab initio lattice dynamics of sapphire. *Phys. Rev. B* **2000**, *61*, 8625. [[CrossRef](#)]
13. Marmier, A.; Parker, S.C. Ab initio morphology and surface thermodynamics of $\alpha\text{-Al}_2\text{O}_3$. *Phys. Rev. B* **2004**, *69*, 115409. [[CrossRef](#)]
14. Batyrev, I.G.; Alavi, A.; Finnis, M.W. Equilibrium and adhesion of Nb/sapphire: The effect of oxygen partial pressure. *Phys. Rev. B* **2000**, *62*, 4698. [[CrossRef](#)]
15. Sivasubramanian, K.; Raju, S.; Mohandas, E. Estimating enthalpy and bulk modulus from thermal expansion data—A case study with $\alpha\text{-Al}_2\text{O}_3$ and SiC. *J. Eur. Ceram. Soc.* **2001**, *21*, 1229–1235. [[CrossRef](#)]
16. Liu, Q.J.; Liu, Z.T.; Chen, J.C.; Feng, L.P.; Tian, H.; Zeng, W. Structural and electronic properties of cubic SrHfO_3 surface: First-principles calculations. *Appl. Surf. Sci.* **2012**, *258*, 3455–3461. [[CrossRef](#)]
17. Chen, G.; Hou, Z.; Gong, X. Structural and electronic properties of cubic HfO_2 surfaces. *Comput. Mater. Sci.* **2008**, *44*, 46–52. [[CrossRef](#)]
18. Li, X.; Hui, Q.; Shao, D.Y.; Chen, J.J.; Li, C.M.; Cheng, N.P. Stability and electronic structure of MgAl_2O_4 (111) surfaces: A first-principles study. *Comput. Mater. Sci.* **2016**, *112*, 8–17. [[CrossRef](#)]
19. Liu, P.L.; Siao, Y.J. Ab initio study on preferred growth of ZnO. *Scr. Mater.* **2011**, *64*, 483–485. [[CrossRef](#)]
20. Segall, M.; Lindan, P.J.; Probert, M.A.; Pickard, C.; Hasnip, P.; Clark, S.; Payne, M. First-principles simulation: Ideas, illustrations and the CASTEP code. *J. Phys.* **2002**, *14*, 2717. [[CrossRef](#)]
21. Søndergård, E.; Kerjan, O.; Barreateau, C.; Jupille, J. Structure and growth of titanium buffer layers on Al_2O_3 (0001). *Surf. Sci.* **2004**, *559*, 131–140. [[CrossRef](#)]
22. Kenny, S. Philos. Ab initio modelling of alumina. *Mag. Lett.* **1998**, *78*, 469–476. [[CrossRef](#)]
23. Gundiah, G.; Deepak, F.; Govindaraj, A.; Rao, C. Carbothermal synthesis of the nanostructures of Al_2O_3 and ZnO. *Top. Catal.* **2003**, *24*, 137–146. [[CrossRef](#)]
24. Gundiah, G.; Govindaraj, A.; Rao, C. Nanowires, nanobelts and related nanostructures of Ga_2O_3 . *Chem. Phys. Lett.* **2002**, *351*, 189–194. [[CrossRef](#)]

